PHILOSOPHICAL TRANSACTIONS OF THE ROYAL SOCIETY A MATHEMATICAL PHYSICAL & ENGINEERING SCIENCES

Degassing and crystallization of ascending andesite and dacite

Kathy Cashman and Jon Blundy

Phil. Trans. R. Soc. Lond. A 2000 **358**, 1487-1513
doi: 10.1098/rsta.2000.0600

THE ROYAL SOCIETY

Degassing and crystallization of ascending andesite and dacite

By Kathy Cashman[1] and Jon Blundy[2]

[1]*Department of Geological Sciences, University of Oregon, Eugene, OR 97403-1272, USA*
[2]*CETSEI, Department of Earth Sciences, University of Bristol, Bristol BS8 1RJ, UK*

The prevalence of andesitic and dacitic volcanic eruptions over the past 20 years has led to a new appreciation of processes typical of magmas of intermediate composition. Extensive syn-eruptive crystallization, driven by decompression and volatile exsolution, is one such process. A water-saturated melt that is decompressed isothermally from its liquidus must crystallize in response to the diminishing capacity of the melt to retain volatiles (particularly H_2O). Only rapid magma ascent allows such a melt to reach the Earth's surface without crystallizing. Intermediate rates of ascent permit varying amounts of syn-eruptive crystallization, which in turn changes magma rheology and affects continued magma progress toward the surface. Feedback among magma decompression, vesiculation, and crystallization is poorly understood, particularly with regard to the kinetics of crystallization.

Here we present two complementary approaches to the study of syn-eruptive, degassing-induced crystallization. The first involves projection of matrix glass compositions onto the well-understood Qz–Ab–Or ternary, which allows relative (quartz-undersaturated melt) or absolute (quartz-saturated melt) determination of magma equilibration (or 'closure') pressure. We show that glass composition (groundmass crystallinity) changes as a function of decompression rate, and that either very slow ascent or rapid ascent followed by arrest and shallow cooling can lead to extensive cotectic precipitation of quartz + feldspar. The second approach involves quantification of plagioclase textures, which provides a direct measurement of the relative importance of crystal nucleation and growth (J/G). This parameter can, in turn, be linked to the effective undercooling (supersaturation) experienced during decompression. Finally, we use phenocryst melt inclusion data to suggest that a substantial amount of *phenocryst* crystallization may also be explained by decompression of water-saturated melt.

Keywords: degassing; crystallization; andesite/dacite volcanoes; Mt St Helens; Pinatubo

1. Introduction

Volcanoes erupt in different ways: explosive and effusive, sustained and intermittent. An outstanding problem in modern volcanology is the prediction of anticipated eruption style from precursory activity, and of transitions in style once an eruption is initiated. Central to this problem is the need for improved understanding of the

chemical and physical changes that magmas 'experience' as they ascend toward the Earth's surface, changes that include exsolution of dissolved volatiles, gas escape, and degassing-induced crystallization of the melt. Here we review one aspect of this problem, namely crystallization that occurs during decompression as a consequence of volatile exsolution. We demonstrate that crystallization is an unavoidable consequence of decompression of a water-saturated melt, and that andesitic magmas, with their high volatile contents and moderate melt viscosities, are particularly susceptible to extensive decompression-driven crystallization. Changes in magma rheology, caused by both volatile loss and crystallization, may in turn play a crucial role in modulating the rate, style and duration of eruptive activity.

2. Background

Recent eruptions of Mt St Helens (USA; 1980–1986), Redoubt (USA; 1989–1990), Mt Pinatubo (Phillipines; 1991), Unzen (Japan; 1991–1993), Mt Spurr (USA; 1992) and Soufrière Hills (Montserrat; 1995–present) illustrate the extent to which magma rise both controls and is affected by the physical consequences of decompression (Cashman 1988, 1992; Geschwind & Rutherford 1995; Nakada *et al.* 1995; Wolf & Eichelberger 1997; Gardner *et al.* 1998*a*; Young *et al.* 1998; Hammer *et al.* 1999; Nakada & Motomura 1999; Melnik & Sparks 1999). In particular, both the density and groundmass crystallinity of eruptive products are inversely correlated with rates of magma ascent. This correlation can be directly attributed to the times available for gas loss (Jaupart 1998) and degassing-induced crystallization (Hammer *et al.* 1999).

Water exsolution during decompression causes an increase in both the liquidus temperature of a magma and the stability of anhydrous mineral phases (particularly plagioclase). Thus, given sufficient time, the melt will crystallize. The effect of water on the stability and composition of plagioclase is well documented (Burnham 1979; Johannes 1980), and is illustrated in several recent experimental studies on mafic to intermediate melt compositions (Sisson & Grove 1993*a*, *b*; Grove *et al.* 1997; Blatter & Carmichael 1998; Moore & Carmichael 1998). Figure 1 shows a phase diagram for a water-saturated andesite (62% SiO_2; from Moore & Carmichael (1998)). At high pressures (greater than 200 MPa) and moderate temperatures (950 °C), the melt is close to its liquidus, with hornblende the only stable phase. With decreasing pressure (and dissolved water content), plagioclase, magnetite and pyroxene join the crystallizing assemblage. By 100 MPa, hornblende is no longer stable and plagioclase is the dominant phase. At 0.1 MPa and 950 °C, the melt is undercooled by more than 200 °C relative to its liquidus temperature. Thus the simple act of isothermal magma decompression and degassing generates an enormous driving force for crystallization, particularly of plagioclase. The extent to which this crystallization proceeds, however, will depend on the effective undercooling generated by the relative rates of decompression and crystallization, and the time available before quenching.

Below we use published data from several recent andesitic and dacitic eruptions (56–68 wt% SiO_2) to illustrate the use of both glass chemistry and crystal textures to interpret magma decompression paths. Matrix glass compositions track changes in groundmass crystallinity, and can be used to determine the pressure at which glass and crystals last attained equilibrium (Blundy & Cashman 2000). Microlite textures record the effective undercooling generated during ascent and temporary storage.

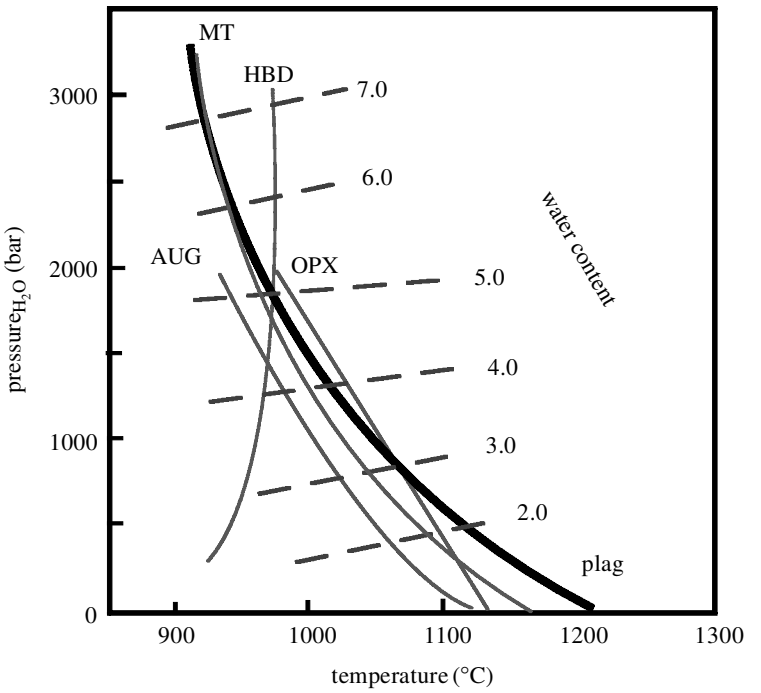

Figure 1. Phase diagram for a hydrous andesitic melt (from Moore & Carmichael 1998). Note particularly the large change in plagioclase liquidus temperature with decreasing pressure and H_2O content.

When magma ascends slowly, the kinetics of hornblende breakdown, a special form of degassing-induced crystallization, can also be used to estimate ascent rate (reviewed elsewhere—see, for example, Rutherford & Hill 1993; Devine *et al.* 1998*a*). Finally, we analyse possible consequences of decompression-driven crystallization for generating phenocryst, in addition to microlite, assemblages, and speculate on the implications of extensive decompressive crystallization for the nature of magma reservoirs beneath andesitic volcanoes.

3. Glass compositions

Matrix glass compositions provide a direct measure of the extent to which crystallization occurs during magma ascent. As matrix glass in pyroclasts of silicic andesite and dacite compositions is commonly rhyolitic, the well-characterized haplogranitic system provides an experimental context for the interpretation of melt evolution paths (Blundy & Cashman 2000). When viewed in this light, the typical evolution of matrix glass to extremely SiO_2-rich (more than 77 wt% on an anhydrous basis) compositions *requires* that much of this crystallization occur at very low pressures (less than 100 MPa).

(*a*) *The haplogranitic system*

Low-pressure phase relations are poorly defined for natural and synthetic silicic systems because of difficulties inherent in experiments on viscous melts (Schairer

1950). However, phase relations in the haplogranite system quartz–albite–orthoclase (Qz–Ab–Or) are well constrained for water-saturated conditions at pressures between 50 and 500 MPa (Tuttle & Bowen 1958; figure 2*a*), and for water-undersaturated conditions at 200 and 500 MPa (Holtz *et al.* 1992*a*). The location of the 0.1 MPa silica–feldspar cotectic, which represents the maximum possible Qz-content of a haplogranitic (anorthite-free) feldspar-saturated liquid, can be approximated from the experiments of Schairer (1950; dashed line in figure 2*a*). At pressures less than 500 MPa, the Qz–Ab–Or system is characterized by two primary phase volumes (silica and feldspar) separated by a curved cotectic. The location of the cotectic, and its minimum, shift systematically towards Qz with decreasing water pressure. At the same time, the temperature of the minimum increases rapidly from 680 °C at 200 MPa to *ca.* 950 °C at 0.1 MPa.

Phase relations in the system Qz–Ab–Or can be used to quantify the effect of decompression-driven crystallization on water-saturated melt compositions (Tuttle & Bowen 1958; figure 2*b*). Melt undergoing isothermal (800 °C) decompression evolves away from the Ab apex as plagioclase crystallizes, until the melt attains silica-saturation (at 50 MPa in the example shown in figure 2*b*). With further decompression the melt composition evolves away from the Qz–Ab binary towards the ternary minimum at still lower pressures. Crystallization ceases when the melt attains its solidus at 30 MPa. In real systems, decompression may involve either adiabatic cooling or heating through crystallization, and thus crystallization paths may deviate from this simple scenario.

To apply these results to natural matrix glass compositions, we must account for the effect of components not present in haplogranites. In particular, anorthite (An), a ubiquitous normative component of natural glasses, substantially displaces the position of the silica–feldspar cotectic to higher Qz contents (Yoder 1968; Johannes & Holtz 1996). The empirical projection scheme of Blundy & Cashman (2000), using data from water-saturated experiments involving Qz, Ab, An and Or, allows us to account for a small amount of normative An (less than 20 wt%):

$$\mathrm{Qz}' = \mathrm{Qz_n} \times (1 - 0.03\mathrm{An} + 6 \times 10^{-5}[\mathrm{Or_n} + \mathrm{An}] + 10^{-5}[\mathrm{Ab_n} \times \mathrm{Or_n} \times \mathrm{An}]), \quad (3.1\,a)$$

$$\mathrm{Or}' = \mathrm{Or_n} \times (1 - 0.07\mathrm{An} + 10^{-3}[\mathrm{Qz_n} \times \mathrm{An}]), \quad (3.1\,b)$$

$$\mathrm{Ab}' = 100 - \mathrm{Qz}' - \mathrm{Or}'. \quad (3.1\,c)$$

Here the subscript 'n' refers to normative Qz, Or and Ab normalized to 100%, and the prime refers to projected values. We assume that the effect of An on liquidus temperatures is modest (*ca.* 30 °C (Johannes & Holtz 1996)). We have also made no attempt to include the effects of normative corundum (Cor) on phase relations (Holtz *et al.* 1992*b*), and thus our projection is restricted to compositions with not more than 1 wt% normative Cor.

Projected compositions may be used to measure the effective pressure at which kinetic factors inhibit crystal growth and the melt chemistry is frozen in, a pressure that we refer to as the 'closure' pressure (P_c). For isothermal ascent, P_c is controlled by the extent to which decompression-driven crystallization can achieve equilibrium conditions during magma ascent, which, in turn, will be dictated by both the time available and the kinetics of crystal nucleation and growth.

The effect of varying decompression time is illustrated by experiments on pumice from the 18 May 1980 eruption of Mt St Helens (Geschwind & Rutherford 1995).

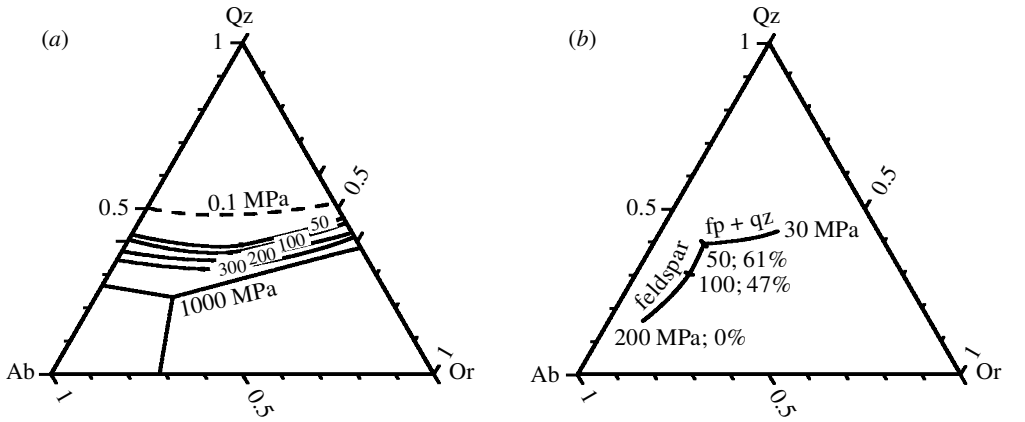

Figure 2. (*a*) Water-saturated phase relations in the haplogranitic system (from Tuttle & Bowen 1958). (*b*) Melt composition and crystallinity (%; in italic) changes that occur when an H_2O-saturated haplogranitic melt at 800 °C is decompressed isothermally from 200 MPa (from Blundy & Cashman 2000).

Samples saturated with H_2O at either 200 or 160 MPa were decompressed at a constant rate to 2 MPa over times ranging from 1 to 192 h, with subsequent annealing for up to 686 h. Resultant glass compositions have been converted to Qz′–Ab′–Or′ plotting parameters (cf. equation (3.1)) and contoured for decompression time (figure 3*a*). The primary effect of increasing decompression time is to increase the value of Qz′ in the residual melt (figure 3*b*), which changes from 0.24 in the rapidly decompressed sample to more than 0.37 in charges decompressed over times in excess of *ca.* 120 h (decompression rates of *ca.* 1 MPa hr^{-1}). An implication of this work is that silica-rich (more than *ca.* 77 wt% SiO_2) glass compositions (i.e. those with low P_c values) can be produced only in magmas that have *equilibrated* at shallow pressures, either through sufficiently slow magma ascent or through temporary near-surface magma arrest before eruption (see below).

(*b*) *Examples from recent eruptions*

Matrix glass compositions have been determined for the products of several recent eruptions, and allow us to use the projection described above to evaluate the effect on glass composition of various pre- and syn-eruptive decompression and crystallization paths. We have chosen to examine eruptions of Mt Pinatubo, Phillipines (1991), Mt St Helens, USA (1980–1986), Unzen, Japan (1991–1995) and Soufrière Hills, Montserrat (1995–present) in detail, as these eruptions span a range of bulk composition (60–68% SiO_2) and eruptive style (explosive to effusive). Additionally, all have detailed observational records.

(i) *Mount Pinatubo*

The eruption of Mt Pinatubo, Phillipines, on 15 June 1991, was the largest and most powerful eruption of recent decades. Events leading up to the climactic eruption included 13 surge-producing events, all of short duration (4–25 min). Both eruptive intensity and repose interval between successive events decreased with time, leading

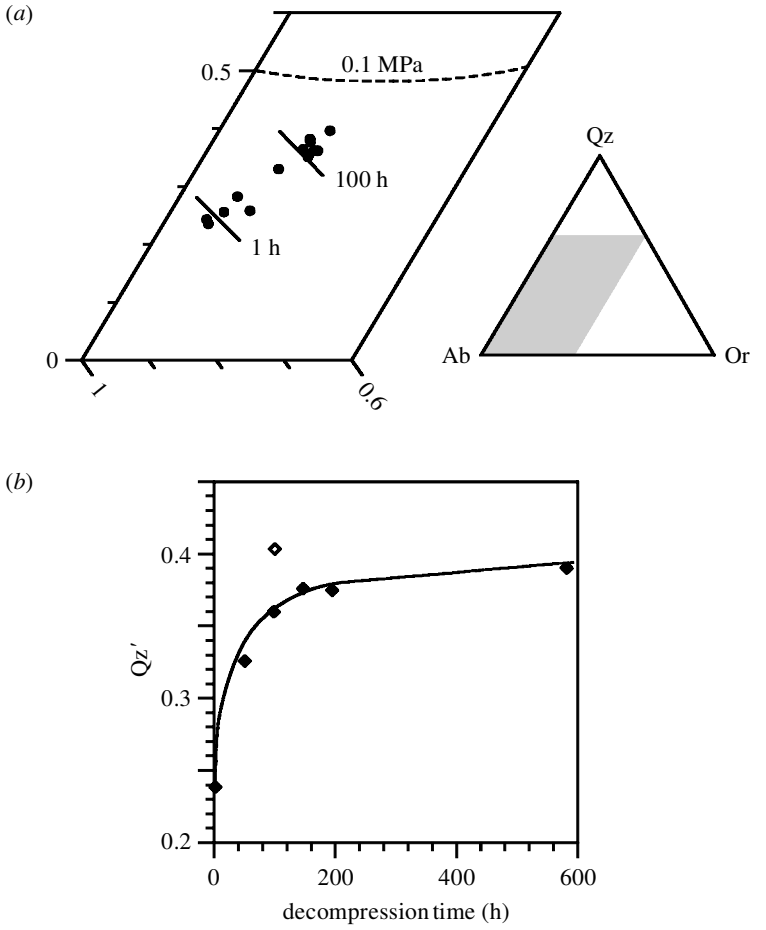

Figure 3. Glass compositions in samples from decompression experiments (900 °C, 160 to 2 MPa) on pumice from Mt St Helens (from Geschwind & Rutherford 1995). (*a*) Projection of glass compositions on Qz–Ab–Or ternary, as described in the text. Data are contoured for duration of decompression. (*b*) Qz′ of experimental glass decompressed from 160 to 2 MPa, as a function of decompression time (in hours).

Hoblitt *et al*. (1996) to suggest that the preclimactic eruptive activity was modulated by a balance between the pressurization rate from below and the rate of depressurization by magma expulsion during precursory events. The mismatch between these two time-scales resulted in magma residence at shallow levels within the conduit, which in turn resulted in decompression-driven crystallization (Hammer *et al*. 1999).

The dominant product of the climactic eruption was low-density, compositionally homogeneous dacite (68% SiO_2) containing up to 47% phenocrystic quartz, feldspar, hornblende, pyroxene, oxides and anhydrite (Pallister *et al*. 1996; Bernard *et al*. 1996). Eruption temperatures were low (780 °C) and initial water content of the melt high (greater than 6 wt%), indicating that the magma was water-saturated at its storage pressure of *ca*. 220 MPa (Rutherford & Devine 1996). The matrix glass composition (in equilibrium with both feldspar and quartz phenocrysts) projects onto the Qz–Ab–Or ternary at a pressure slightly less than 200 MPa (figure 4*a*).

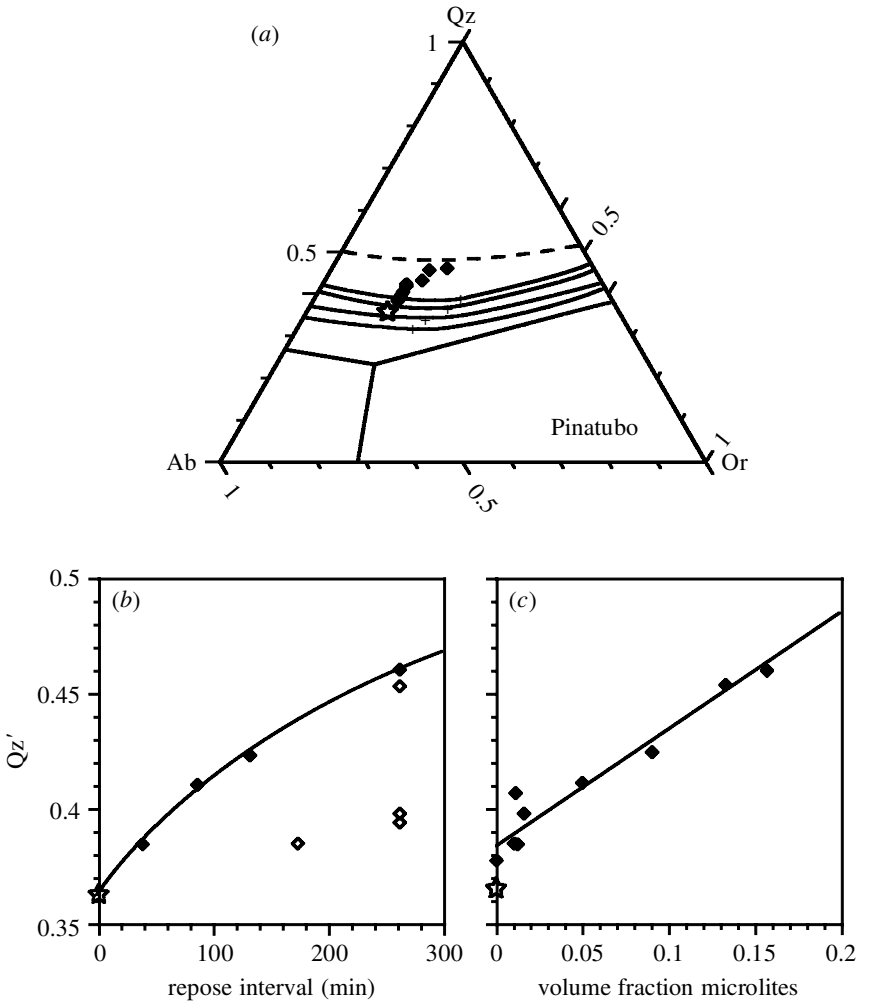

Figure 4. Glass compositions in pre-climactic (solid diamonds) and climactic white pumice (open star) from the 1991 eruption of Mt Pinatubo (data from Rutherford & Devine 1996; Hammer *et al*. 1999). (*a*) Projection on Qz–Ab–Or ternary. (*b*) Relationship of Qz′ to repose interval. (*c*) Relation of Qz′ to plagioclase microlite volume fraction (ϕ). Only those analyses with normative Cor of less than 1 wt% were used in these plots (see text).

Dacite pyroclasts from pre-climactic events are compositionally identical to the climactic pumice but have uniformly low H_2O contents (1.3–1.7 wt%, in equilibrium at 6–16 MPa (Hammer *et al*. 1999)) and highly variable densities (700–2580 kg m^{-3}; Hoblitt *et al*. 1996). These characteristics may be explained by rapid magma decompression, volatile exsolution and arrest of the magma at a shallow level during each surge event, followed by inter-eruptive gas escape and crystallization (Hammer *et al*. 1999). The least evolved glasses in surge pyroclasts project onto the Qz–Ab–Or ternary at slightly lower pressures (less than *ca*. 100 MPa) than matrix glass from the climactic pumice (figure 4*a*). The most evolved glass compositions approach the 0.1 MPa cotectic, consistent with equilibration of these samples at low pressures. A

single highly crystalline (20% microlites) sample shows slight enrichment in Or′, as expected for minor cotectic precipitation of feldspar + quartz (e.g. fig. 4 of Hammer *et al.* 1999).

The glass compositions preserved in individual pyroclasts can be used to monitor inter-eruptive crystallization in response to rapid decompression. Figure 4*b* shows that the relatively cool (780 °C) rhyolitic melt crystallized rapidly in response to decompression (in hours). Interestingly, microlite-free glass from clasts in the surge deposits has higher Qz′ values than that of the climactic white pumice, suggesting that minor phenocryst rim growth may permit some crystallization before nucleation of microlites. Following Hammer *et al.* (1999), we take the repose interval as the relevant time-scale, and use Qz′ to track melt composition (figure 4*b*). The range in Qz′ within individual deposits probably reflects tapping of a vertical conduit (variable decompression histories), thus we use the maximum observed Qz′ to define the rate of change in glass composition ($dQz'/dt \approx 0.02\,hr^{-1}$). This rate of glass evolution is substantially faster than in the experiments of Geschwind & Rutherford (1995; $dQz'/dt \approx 0.001\,hr^{-1}$, figure 3*b*). The difference may reflect differences in the decompression paths: 'instantaneous' decompression followed by low pressure annealing at Pinatubo contrasted with steady decompression in the experiments. Comparison of glass data with modal data from Hammer *et al.* (1999) shows that the observed increases in Qz′ from 0.37 to more than 0.46 record an increase in groundmass crystallinity from 0 to 17% (figure 4*c*). The observed Qz′ range at low crystallinities may reflect different amounts of phenocryst rim growth or difficulties in measuring small percentages of microlites.

(ii) *Mt St Helens, WA*

The 1980–1986 eruption of Mt St Helens included both explosive production of dacitic pumice and later effusive growth of a composite dacite dome (Scandone & Malone 1985; Swanson *et al.* 1987). The climactic eruption of 18 May 1980 was preceded by two months of precursory activity, including emplacement of a 'cryptdome' in the volcanic edifice. The magma originally contained melt with *ca.* 4.6 ± 1.1 wt% H_2O (Rutherford *et al.* 1985) and *ca.* 33% phenocrysts of hornblende, plagioclase, pyroxene and oxides (Kuntz *et al.* 1981). Pumice deposits from 18 May contain abundant low-density (white) clasts with microlite-free groundmass glass, smaller amounts of grey, microlite-bearing pumice (Criswell 1987; Klug & Cashman 1994) and moderate- to high-density cryptodome dacite (Hoblitt & Harmon 1993).

Groundmass glass compositions vary with clast type. White pumice has matrix glass with Qz′ = 0.23–0.24 (figure 5*a*), the equilibrium composition for 900 °C and more than 160 MPa (Rutherford *et al.* 1985; Rutherford & Devine 1988). In contrast, blast dacite and grey pumice samples have glass compositions with Qz′ = 0.48 and P_c values close to 0.1 MPa. The high values of Qz′ are most easily explained by shallow arrest of magma in the cryptodome and shallow conduit before the climactic eruption (Hoblitt & Harmon 1993). Subsequent explosive eruptions during the summer of 1980 produced pumice clasts with a range of density, phenocryst content, and glass composition (Kuntz *et al.* 1981; Melson 1983; Geschwind & Rutherford 1995). Matrix glass compositions also vary considerably in these samples, with $0.25 \leqslant Qz' \leqslant 0.46$ (figure 5*a*). Several of the explosive eruptions were followed by dome extrusions, and after October 1980 eruptions were almost exclusively effusive

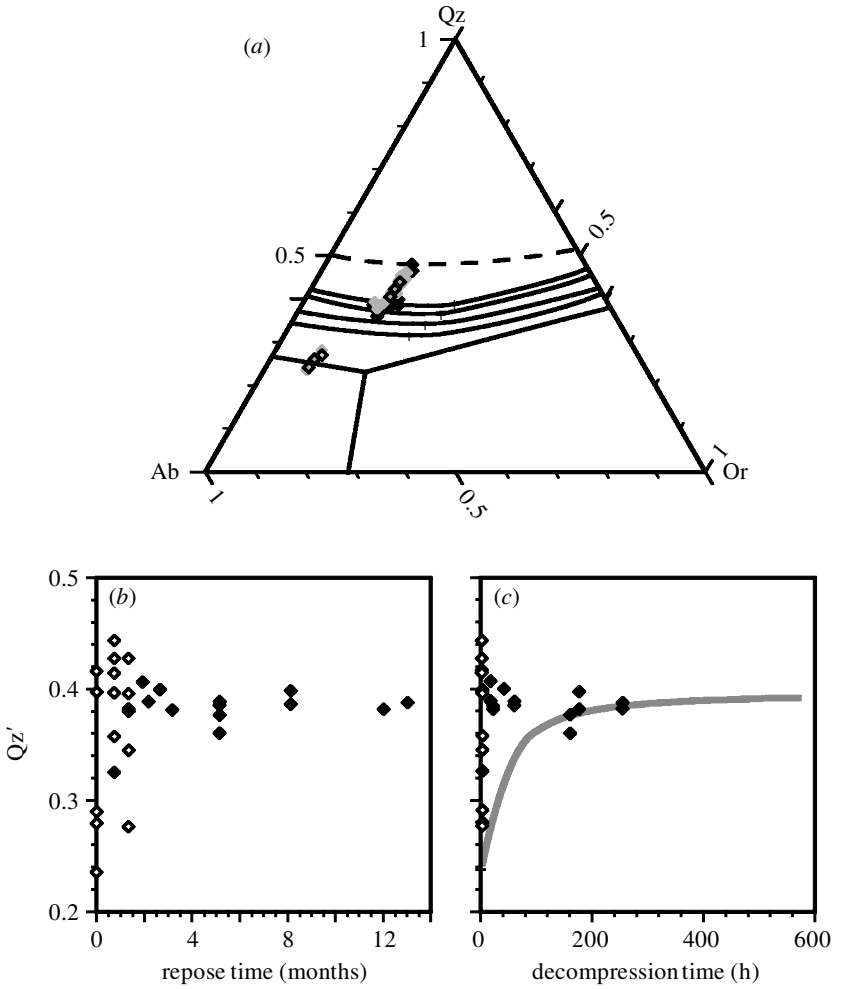

Figure 5. Homogeneous glass compositions in clasts from the 1980–1986 eruption of Mt St Helens, 1980–1986. (*a*) Projection of glass data on Qz–Ab–Or ternary; 18 May 1980 (open diamonds), summer 1980 (light grey diamonds), late 1980–1986 dome lavas (black diamonds). (*b*) Relationship of Qz′ to repose time (in months). (*c*) Relationship of Qz′ to estimated decompression time (based on Scandone & Malone 1985; Endo *et al*. 1990; Geschwind & Rutherford 1995). Curve is from data of Geschwind & Rutherford (1995), as shown in figure 3*b*.

(Moore *et al*. 1981). Dome lavas have higher phenocryst and microphenocryst contents than explosively erupted pyroclasts (Cashman & Taggart 1983; Cashman 1992), and the matrix glass compositions of lava dome samples are correspondingly evolved ($Qz' > 0.38$; figure 5*a*). While initially believed to represent progressive tapping of a magma reservoir zoned in volatile content (Melson 1983), the observed variability in glass composition has subsequently been interpreted to reflect variable degrees of decompression-driven crystallization (Merzbacher & Eggler 1984; Cashman 1992; Geschwind & Rutherford 1995).

When and where does the groundmass crystallization occur? If crystallization occurred primarily between eruptive episodes (Cashman 1992), the glass compo-

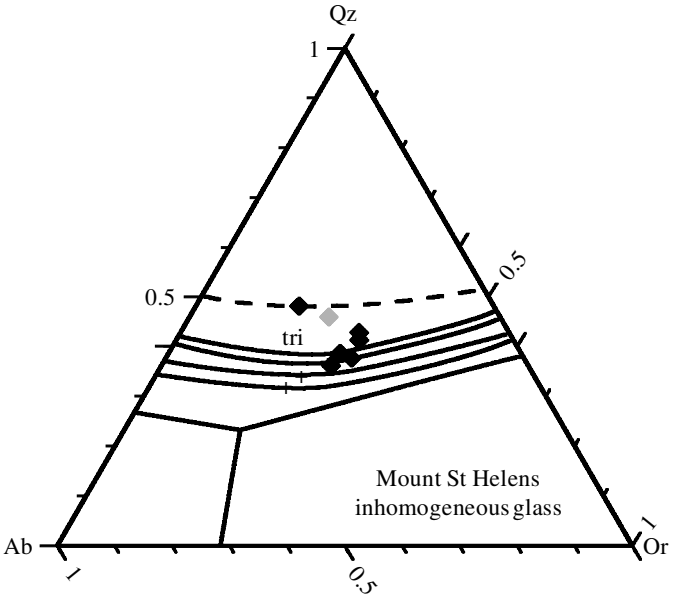

Figure 6. Projection of inhomogeneous glass compositions from Mt St Helens onto Qz–Ab–Or ternary. Composition of a tridymite-bearing sample shown in grey and labelled tri. Ternary minimum compositions (from figure 2*a*) are shown as crosses.

sition should correlate with repose duration, as seen at Pinatubo. Figure 5*b* shows a poor correlation between these parameters. Instead, glass in pyroclasts (open symbols) from explosive eruptions preceded by short repose intervals (weeks) shows a greater range and higher maximum Qz′ than observed in dome lavas (filled symbols) with longer repose intervals (months). If instead crystallization was syn-eruptive (Geschwind & Rutherford 1995), glass compositions should correlate with rates of magma decompression. Syn-eruptive decompression time-scales can be approximated using estimated magma ascent velocities (from Scandone & Malone 1985; Endo *et al*. 1990; Geschwind & Rutherford 1995), and assuming that decompression is linearly related to depth (although this is clearly an over-simplification, particularly for explosive eruptions (Gilbert & Sparks 1998; Cashman *et al*. 1999; Melnik & Sparks 1999)). A plot of the Qz′ dependence on decompression time (figure 5*c*) shows that this parameter is also a poor predictor of glass composition, particularly in the pyroclasts. When considered in the light of the preclimactic pyroclasts from Pinatubo, these data suggest that evolution of high Si-glass in explosive pyroclasts required at least a two-stage decompression history, with rapid decompression during an eruptive event followed by crystallization at shallow levels before pyroclast formation in the next eruption. The apparent insensitivity of glass composition to repose interval indicates that crystallization was rapid (less than the minimum repose interval of one week) and that the actual glass composition of each clast probably reflects its pre-eruptive location in the conduit.

Lava samples from episodic dome extrusions have relatively homogeneous glass compositions, despite highly variable repose durations (less than 2 to more than 12 months) and decompression times (less than 20 to more than 200 h). This homogeneity may also reflect complex but repeatable decompression paths involving both inter-

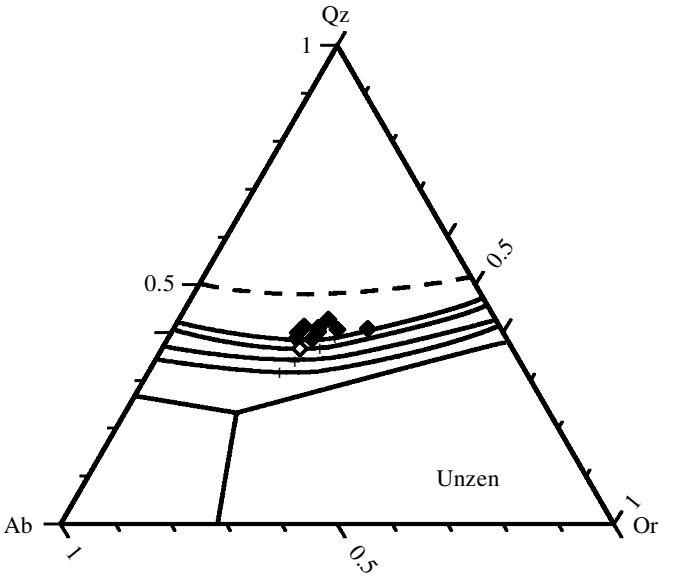

Figure 7. Projection of glass compositions from 1991 to 1995 Unzen lavas onto Qz–Ab–Or ternary (data from Nakada *et al*. 1995; Nakada & Motomura 1999).

and syn-eruptive crystallization (see textural data below). In contrast continuous endogenous dome growth in 1983 produced lava characterized by a groundmass silica phase. These samples have glass compositions that are highly evolved ($Qz' = 0.46$) and displaced toward the Qz′–Or′ join, lying close to the water-saturated minimum composition (figure 6). Glass compositions yield moderate closure pressures (not less than 30 MPa) that are not compatible with expected equilibration to low pressures. This discrepancy may reflect non-equilibrium crystallization paths, particularly if crystallization initiated with a cotectic (feldspar + quartz) assemblage, rather than crystallizing feldspar alone until reaching the appropriate cotectic.

(iii) *Unzen volcano*

The 1991–1995 eruption of Unzen volcano was primarily effusive. Dome lavas contain on average 64.5 wt% SiO_2 bulk and 23–28% phenocrysts of plagioclase, hornblende, biotite, quartz and magnetite, although both the bulk magma composition and phenocryst content varied with eruption rate (Nakada *et al*. 1995; Nakada & Motomura 1999). Abundant evidence for phenocryst disequilibrium with the melt has been variously interpreted as the product of mixing two magmas (Venezsky & Rutherford 1999) or incorporation of dioritic xenocrysts into parental rhyolitic magma (Nakada & Motomura 1999).

Projection of glass compositions onto the Qz–Ab–Or ternary shows a range of Qz′ values and corresponding P_c that appear to correlate with effusion rate (as noted by Nakada *et al*. 1995; Nakada & Motomura 1999). Pumice from an early explosive event (volumetric eruption rate is *ca*. 5 $m^3\ s^{-1}$) has 25% microlites (Nakada & Motomura 1999) and glass $Qz' = 0.37$ ($P_c \approx 100$ MPa), close to pressure estimates for pre-eruptive magma storage (Nakada *et al*. 1995; Sato *et al*. 1999). Lower rates of magma effusion from mid-1991 to mid-1994 produced lava domes containing abun-

dant groundmass plagioclase (33–43%; Nakada & Motomura 1999). Glass in these samples is more highly evolved than in pumiceous samples ($Qz' = 0.39$–0.43), and shows minor Or′-enrichment indicative of incipient cotectic crystallization (figure 7). After mid-1994, the magma flux was very low (less than 0.1 $m^3\ s^{-1}$), and endogenous dome growth was accompanied by extrusion of lava spines with low Fe–Ti oxide temperatures, high groundmass crystallinities (50%) and 'partial devitrification' (quartz precipitation?) of the groundmass (Nakada & Motomura 1999). These features indicate that shallow cotectic precipitation of quartz and feldspar occurred during very slow ascent, as seen at Mt St Helens.

Minimum crystallization times can be estimated for Unzen samples, again assuming a linear relationship between ascent velocity and decompression rate. If the Unzen magma attained water saturation at 4 km (Nakada *et al.* 1995) and the maximum rate of magma ascent was 0.01 $m\ s^{-1}$ (Nakada & Motomura 1999), the minimum decompression time for the pumiceous sample was *ca.* 100 h. High Qz' values for dome samples erupted at lower effusion rates thus require decompression over substantially longer times. P_c values of less than 50 MPa suggest equilibrium to shallow (less than 1 km) levels, particularly if the conduit sustained substantial overpressures (up to 10 MPa; Nakada & Motomura 1995). Interestingly, this is also the location of syn-eruptive seismic activity and of the source depths of early Vulcanian explosions (0.6–0.8 km; Nakada *et al.* 1999).

(iv) *Soufrière Hills volcano, Montserrat*

Lava produced during the 1995–present eruption of the Soufrière Hills volcano, Montserrat can be used to examine syn-eruptive crystallization in a slightly more mafic bulk composition (*ca.* 60 wt% SiO_2 (Young *et al.* 1998)). This eruption has also been predominantly effusive, with eruption rates increasing from *ca.* 0.2 $m^3\ s^{-1}$ in late 1995 to more than 10 $m^3\ s^{-1}$ in early 1997 (Sparks *et al.* 1998). As at Mt St Helens and Unzen, explosive activity occurred when magma flux was high. The andesite magma has *ca.* 40% phenocrysts of plagioclase, hornblende, orthopyroxene, Fe–Ti oxides, and resorbed quartz. The original H_2O content of the melt is inferred to be 3.8–4.8 wt%, with magma storage at 115–130 MPa and *ca.* 830 °C, although there is evidence for reheating to *ca.* 880 °C (Barclay *et al.* 1998; Devine *et al.* 1998*a*, *b*).

Dome lavas have glass compositions (Barclay *et al.* 1998; Devine *et al.* 1998*b*; Murphy *et al.* 2000) that show a range of P_c values when projected onto the Qz–Ab–Or ternary. The least evolved glass ($Qz' = 0.34$) occurs in a pumiceous sample erupted in September 1996 (figure 8*a*). The presence of quartz allows us to bracket P_c between 100 and 200 MPa, consistent with experimental determinations of 130 MPa (Barclay *et al.* 1998). More slowly erupted dome lavas show declining P_c values (to 30–50 MPa) with diminishing magma flux. As at Mt St Helens and Unzen, very low rates of effusion produced lava spines with Or′-enriched glass compositions (figure 8*b*). Variable degrees of Or′-enrichment indicate that these lavas experienced different degrees of cotectic precipitation of feldspar + a silica phase (probably cristobalite (Baxter *et al.* 1999)) at shallow (20–40 MPa) pressures.

(*c*) *Glass summary*

Matrix glass compositions can record small amounts of crystallization. For example, our plotting parameter Qz' changes by 0.03–0.05 for each per cent increase in

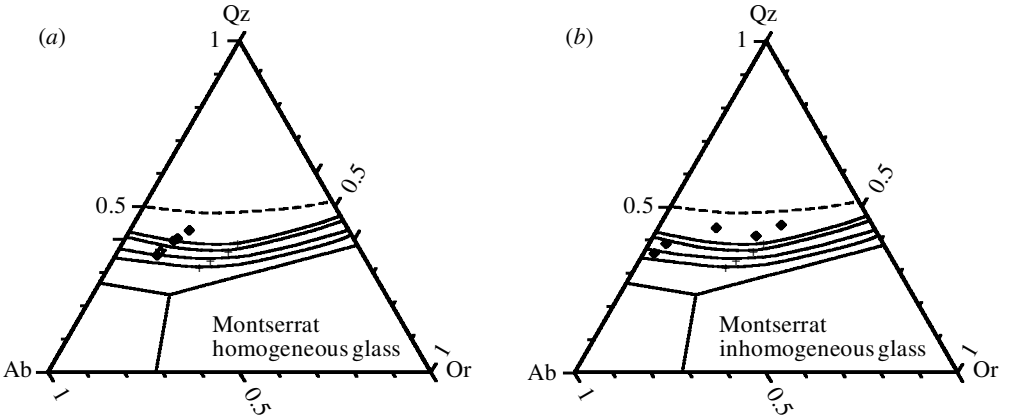

Figure 8. Glass compositions from 1995 to 1997 lavas of Soufrière Hills volcano, Montserrat projected on Qz–Ab–Or ternary (data from Devine *et al*. 1998; Murphy *et al*. 1998; Murphy & Sparks 1999). (*a*) Homogeneous glasses. (*b*) Inhomogeneous glasses.

groundmass crystallinity (based on data from Si-free glasses from Pinatubo and Mt St Helens). Projection of glass compositions onto the Qz–Ab–Or ternary allows determination of actual (quartz-saturated) or relative (quartz-undersaturated) magma storage pressures in rapidly erupted pumiceous samples. Rapid decompression to shallow levels promotes rapid and extensive crystallization, if followed by sufficient time at low pressure to allow crystallization. Such a decompression path can result in highly evolved glass compositions, as seen in pyroclasts from Mount Pinatubo and Mt St Helens. Slower decompression accompanying continuous or episodic extrusion of lava domes (e.g. Mt St Helens, Unzen, and Soufrière Hills) leads to moderately evolved glass compositions ($Qz' > 0.38$) and correspondingly low closure pressures ($P_c = 100$ MPa). Comparison of the products of explosive and effusive eruptions at Mt St Helens suggests that the most evolved glass compositions are formed when decompression to low pressures is rapid, an interpretation supported by experimental data of Hammer & Rutherford (1999). These conclusions point to the need for more experimental data on the effects of decompression path on both the rates and ultimate extent of crystallization.

Shallow arrest of magma, or extremely slow ascent, may also permit extensive co-precipitation of feldspar plus a silica phase and evolution of glass compositions toward the ternary minimum. The observation that glass compositions of dome lavas evolve to and along low-pressure cotectic paths in the Q–Ab–Or system has a number of potentially important implications. The high groundmass crystallinities that result from extensive cotectic precipitation of quartz and feldspar will dramatically change magma rheologies, and may be responsible for the extrusion of Peléean spines as solid plugs. Shallow cotectic crystallization of quartz and feldspar may also contribute to the explosivity of silicic domes, which has been attributed to volatile exsolution resulting from low-pressure crystallization of anhydrous minerals (Sparks 1997; Stix *et al*. 1997). The observed evolution of melt compositions to thermal minima in dome and spine samples suggests that such crystallization may be sufficiently rapid to produce the volatile overpressures required to fuel local dome explosions in response to dome collapse (Alidibirov & Dingwell 1996; Navon *et al*. 1998).

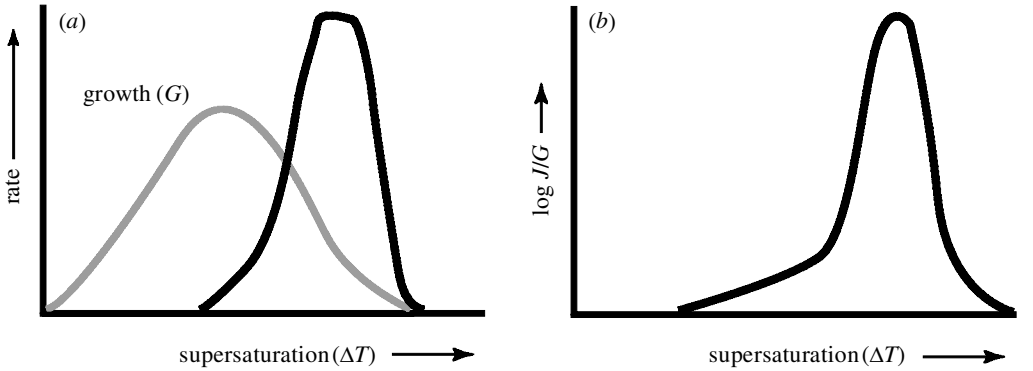

Figure 9. (*a*) Schematic of changes anticipated in rates of crystal nucleation (J) and growth (G) as a function of supersaturation (ΔT). (*b*) Schematic of changes in the parameter J/G as a function of ΔT that would result from the nucleation and growth curves of (*a*).

4. Textural studies

While the composition of matrix glass provides a measure of syn-eruptive crystallization, groundmass textures can be used to determine how that crystallization occurred. Groundmass textures are controlled primarily by rates of crystal nucleation, which vary considerably for different magma decompression paths. Crystal sizes, shapes, and abundance, in turn, control the extent to which increasing crystallinity affects magma rheology. Below we provide a brief overview of crystallization kinetics before presenting some case studies that help to constrain the kinetics of plagioclase crystallization during magma ascent.

(*a*) *Kinetics of crystallization and vesiculation*

Crystallization requires supersaturation, or 'undercooling' (ΔT), of a melt with respect to the saturation temperature (liquidus) of a given crystal phase. Isothermal decompression of water-saturated magma causes the liquidus temperature to increase dramatically (e.g. figure 1), thus causing ΔT to increase. Under near-equilibrium conditions, this increase in ΔT is offset by crystallization that drives the melt to more evolved compositions with lower liquidus temperatures, and hence lower ΔT. The rate of decompression determines the extent to which crystallization is able to keep pace with the imposed ΔT. The overall style of crystallization is thus determined by complex feedback between the decompression path and kinetic constraints on crystal nucleation and growth.

The relative rates of crystal growth and nucleation as a function of ΔT (Lofgren 1980; Kirkpatrick 1981) are shown schematically in figure 9*a*, scaled to reflect the large variations observed in rates of nucleation relative to growth (Cashman 1990, 1993). At moderate ΔTs, new crystals have difficulty nucleating, and crystallization occurs primarily by growth of existing crystals. At large ΔTs, nucleation, and thus the addition of new crystals, dominates. At very large ΔTs, the large driving force for crystallization is countered by limiting rates of diffusion (a consequence of large increases in melt viscosities at low water contents (Hess & Dingwell 1996)), and the melt quenches to glass (i.e. does not crystallize).

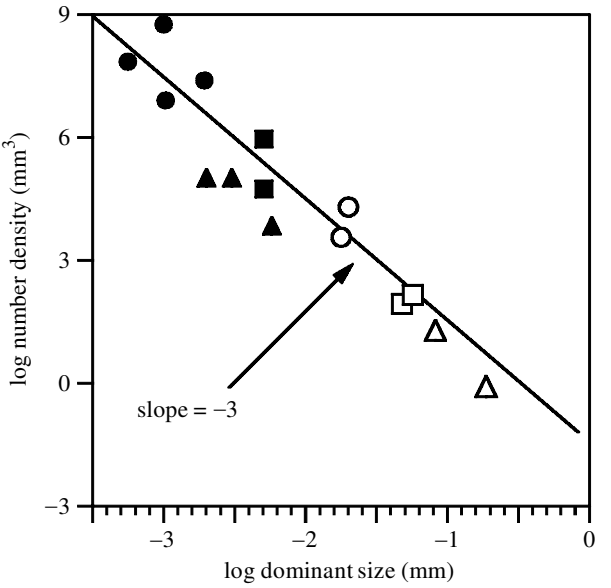

Figure 10. Compilation of data showing the variation in log (crystal number density) versus log (crystal size) predicted by equations (3.1 *a*) and (3.1 *b*). Data from Hammer *et al.* (1999) (filled circles), Gardner *et al.* (1998*a*) (filled triangles), Higgins (1996*a*, *b*) (open triangles), Armienti *et al.* (1994) (open squares), Cashman (1993) (open circles).

The relative importance of nucleation and growth during crystallization, in turn, has a profound effect on the resulting crystal textures. Non-dimensionalization of classical expressions (Winkler 1949; Shaw 1965; Brandeis & Jaupart 1987; Marsh 1998) shows that the average crystal size (L) and crystal number density (N_v, per volume) are related to time-averaged rates of nucleation (J) and growth (G) as

$$L \approx (J/G)^{-1/4}, \tag{4.1 a}$$

$$N_\mathrm{v} \approx (J/G)^{3/4} \approx 1/L^3. \tag{4.1 b}$$

The parameter J/G can, in turn, be related directly to ΔT if appropriate thermodynamic parameters are known (Armienti *et al.* 1994). Predicted variations in J/G with ΔT are shown schematically in figure 9*b* for the nucleation and growth curves of figure 9*a*. Note that the ratio of the two rates (and hence N_v) rises precipitously and peaks sharply at some high ΔT, and then drops rapidly as G starts to dominate the crystallization process. J/G eventually drops to 0 as nucleation ceases, although diffusion ensures that existing crystals may still grow.

Textures in volcanic rocks illustrate the relationship expressed in equation (4.1 *b*). Plagioclase number density and size data from samples spanning a wide range in bulk composition and crystallization conditions approximate a straight line with a slope of −3 when plotted as $\log(N_\mathrm{v})$ versus $\log L$ (figure 10). The 10^{10} range in observed values of N_v indicates that J/G varies by more than 10^{14} in these samples. Thus rock textures, particularly crystal number densities, are extraordinarily sensitive to initial supersaturation (ΔT) conditions.

The extreme variation in N_v illustrated in figure 9 makes it a useful parameter for characterization of groundmass textures. While direct measurement of N_v is difficult

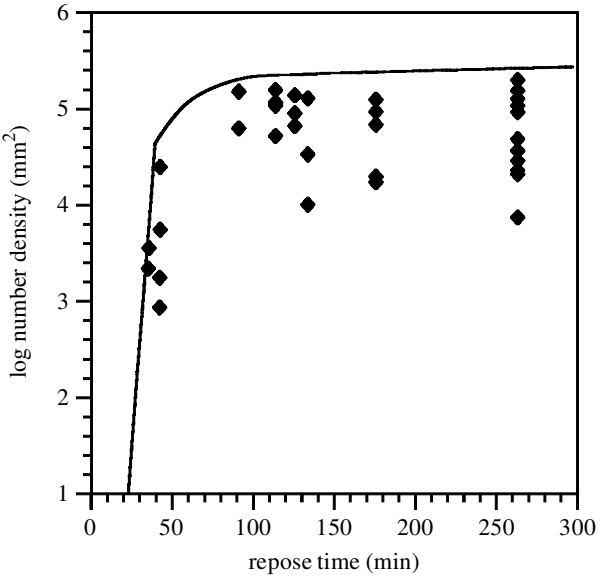

Figure 11. Plagioclase number densities in Pinatubo pre-climactic pumice, shown as a function of repose time. Note that the maximum crystal number increases rapidly, then plateaus after *ca.* 100 min. Data from Hammer *et al.* (1999).

(Manga 1998), areal number density (N_a) and crystal fraction (ϕ_a) can be measured easily and accurately (Hammer *et al.* 1999, 2000; Cashman *et al.* 1999). These two parameters are related through the average crystal area (assumed for simplicity to be L^2) as

$$N_a = \phi_a / L^2. \tag{4.2}$$

Measurements of N_a and ϕ_a in two dimensions may be related to three-dimensional measurements through use of simple stereological assumptions. The area fraction (ϕ_a) is directly equivalent to volume fraction (ϕ; e.g. Chayes 1956), and volumetric number density (N_v) can be calculated (Underwood 1970) as

$$N_v = N_a / L_{av}, \tag{4.3}$$

where the average size (L_{av}) is determined from equation (4.2), noting that $L_{av} = \sqrt{L^2}$. Although more detail can be achieved from measurement of areal or volumetric crystal shapes (Higgins 1994; Hammer *et al.* 1999), orientations (Manga 1998) and size distributions (Cashman 1988, 1992; Armienti *et al.* 1994; Higgins 1996*a*, *b*; Hammer *et al.* 1999), these measurements are time-consuming and few detailed studies have been done. For this reason, we focus here on information provided by the simple measurement of crystal number density; the reader is referred to the references above for details on crystal size distribution studies.

(*b*) *Examples from recent eruptions*

Plagioclase is the most abundant phenocryst and groundmass phase in andesitic and dacitic pyroclasts and lavas. Recent studies of plagioclase microlites show the

Table 1. *Textural data*

volcano	P (MPa)	N_v (mm^{-3})	J/G (mm^{-4})
Pinatubo	6–16	$> 10^9$	$> 10^{12}$
MSH[a] (microlites)	10–30	5×10^7	$> 10^{10}$
MSH (microphenocrysts)	? 100–160	$1–5 \times 10^5$ (max)	$5–40 \times 10^6$
Mt Spurr	?	$10^6–10^7$	$10^8–10^9$

volcano	J ($mm^{-3}\ s^{-1}$)	G ($mm\ s^{-1}$)
Pinatubo	$> 10^5$ (max)	10^{-7}
MSH (microlites)	$> 10^2$ (min)	2×10^{-8} (min)
MSH (microphenocrysts)	0.05–0.2 (max)	10^{-8} (max)
Mt Spurr	15–500	$1.5–50 \times 10^{-8}$

[a] Mt St Helens.

importance of decompression paths for the generation of diverse groundmass textures, while estimated decompression times can be used to constrain decompressive rates of plagioclase nucleation and growth.

(i) *Mt Pinatubo, 1991*

As described in § 3 *b* (i), pyroclasts from the preclimactic eruptions of Mt Pinatubo record the temporal response of melt to rapid decompression followed by crystallization at a constant (shallow) pressure (Hammer *et al.* 1999). All surge deposits with repose intervals in excess of *ca.* 40 min contain a range of clast types (microlite-free to microlite-rich). In these deposits, both maximum groundmass crystallinity (ϕ) and maximum microlite number density (N_a) then increase with further repose duration (figures 4*b* and 11). N_v shows an apparent saturation value of *ca.* $10^9\ mm^{-3}$ ($J/G > 10^{12}\ mm^{-4}$) at repose intervals of not less than 100 min, indicating that most microlites nucleated over the time-interval of 40–100 min. This time-scale yields nucleation rates not less than $10^5\ mm^{-3}\ s$ (table 1) and, using the measured J/G, average growth rates of *ca.* $10^{-7}\ mm\ s^{-1}$. Small increases in bulk crystallinity for longer repose times were accomplished primarily through crystal growth, as indicated by changes in average plagioclase shape (Hammer *et al.* 1999). Such variations in the relative importance of nucleation and growth are consistent with rapid decompression (large ΔT) followed by a gradual approach to equilibrium (diminishing ΔT) with time (figure 9). The high crystal number densities and nucleation rates determined for these samples reflect temporary magma storage between surge events at pressures (effective ΔTs) corresponding to the nucleation maximum for Pinatubo magma (Hammer & Rutherford 1999).

(ii) *1980–1986 eruption of Mt St Helens*

Pyroclasts and lavas from Mt St Helens also show large variations in microlite content and textures. The microlite population is dominated volumetrically by plagioclase, although very small Fe–Ti oxides are ubiquitous and often numerous. Plagioclase microlite textures vary both within individual pyroclastic deposits, and between explosive and effusive eruptive episodes.

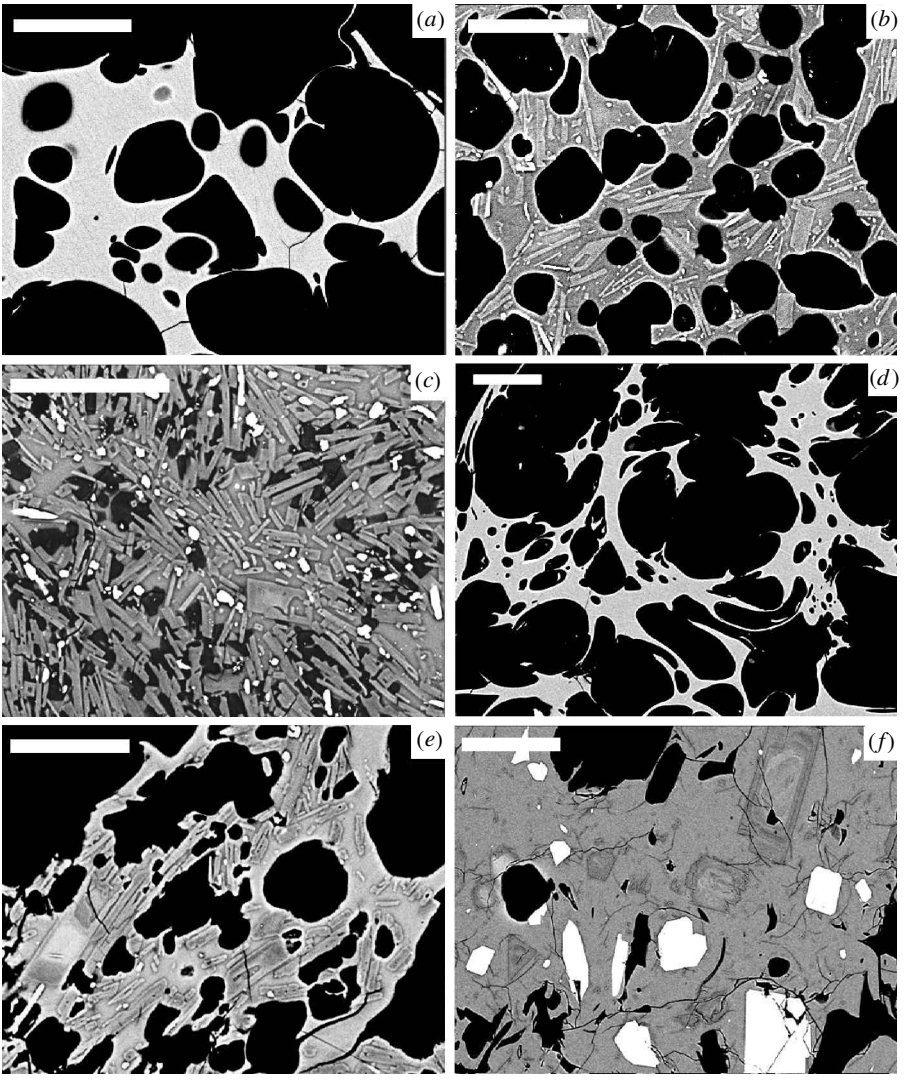

Figure 12. Backscattered electron images of groundmass textures in products of the 1980–1986 Mt St Helens eruption. Glass and plagioclase microlites are grey, pyroxene and oxide microlites are white, silica phases are dark grey and vesicles are black. Scale bar is 20 μm in all images except (*f*), where it is 50 μm. (*a*) 18 May 1980 white pumice; (*b*) 18 May 1980 grey pumice; (*c*) 18 May 1980 cryptodome dacite; (*d*) 22 July 1980 white pumice; (*e*) 12 June 1980 pumice; (*f*) December 1980 dome lava

Tephra produced during the explosive eruptions of 1980 show a range of clast densities (Kuntz *et al.* 1981; Hoblitt & Harmon 1993) that reflects a range of groundmass crystallinities and microlite textures (Klug & Cashman 1994; figure 12*a*–*e*). The explosive eruption of 18 May 1980 produced both microlite-free (white) pumice (figure 12*a*), and grey pumice and cryptodome dacite containing abundant microlites (figure 12*b*,*c*). High microlite number densities in the blast dacite are accompanied by extensive precipitation of groundmass quartz, consistent with magma arrest at

shallow levels. Pyroclasts from later explosive eruptions on 25 May, 12 June, and 22 July 1980 show the same range of groundmass textures (figure 12*d*,*e*). Most clasts also contain microphenocrysts, ubiquitous in later dome lavas, with well-developed oscillatory zoning (figure 12*f*).

Three fundamentally different groundmass textures characterize the explosive pyroclasts, textures that can be related to different J/G regimes shown in figure 9. Microlite-free glass typifies the abundant low-density white pumice. Finely crystalline clasts, such as the cryptodome and grey dacite samples erupted on 18 May have high number densities of small acicular plagioclase microlites and glass compositions that indicate equilibration at shallow levels (10–30 MPa, resulting in ΔTs in excess of 100 °C (Rutherford *et al.* 1985)). The restriction of these two clast types to the explosive eruptions suggests a scenario similar to that described for the preclimactic eruptions of Mt Pinatubo, where rapid decompression to shallow levels is followed by a repose interval during which crystallization occurs, consistent with conclusions based on glass compositions. The shortest repose interval between explosive eruptions was the week separating the 18 May and 25 May eruptions. The lack of correspondence between the repose interval and glass composition suggests, however, that crystallization time-scales may have been substantially shorter. Plagioclase number densities of 5×10^7 mm^{-3} s ($J/G \approx 10^{10}$ mm^{-4}) thus yield a minimum nucleation rate of more than 10^2 mm^{-3} s and growth rates of *ca.* 2×10^{-8} mm s^{-1} (table 1).

The third clast type, which is common in post-18 May pyroclastic deposits, is characterized by a predominance of oscillatory zoned plagioclase microphenocrysts (with or without accompanying microlites). Microphenocryst-bearing pyroclasts had different decompression histories than their microlite-rich counterparts. Microphenocryst number densities are relatively low (not more than 5×10^5 mm^{-3}) and their sizes relatively large (tens of micrometres), both characteristics suggesting crystallization at higher pressures (lower ΔTs) than the microlite-rich samples (e.g. figure 8). Hornblende breakdown rims of non-zero but variable thickness indicate magma residence at pressures lower than 160 MPa, although the time required to generate observed rim thicknesses cannot be determined uniquely without knowledge of the decompression path (Rutherford & Hill 1993). Ubiquitous oscillatory zoning of the microphenocrysts may record either multiple decompression steps or pressure fluctuations imposed on deeper magma during earlier episodic eruptions. The separate microlite population in many samples may reflect late-stage syn-eruptive low-pressure crystallization (Geschwind & Rutherford 1995).

Nucleation and growth rates for microphenocrysts in the 12 June 1980 pyroclasts can be calculated if we assume that crystallization commenced when magma migrated into an intermediate depth storage region during an earlier eruption (either 18 or 25 May). Resultant times of 17–24 days yield nucleation rates of 0.2 mm^{-3} s and growth rates of 1–2 $\times 10^{-8}$ mm s^{-1} (table 1). These rates are similar to those estimated by Cashman (1992) for a sample of the June 1980 lava dome.

Oscillatory zoned plagioclase microphenocrysts are ubiquitous in lava produced by subsequent effusive activity. In addition, these lavas have plagioclase, pyroxene and Fe–Ti oxide microlites, and hornblende phenocrysts in varying stages of breakdown. Lava samples typically have plagioclase number densities of less than 10^5 mm^{-3} that decrease slightly through time (Cashman 1992). If growth rates are similar to those estimated for microphenocryst growth in early pyroclasts (table 1), nucleation rates

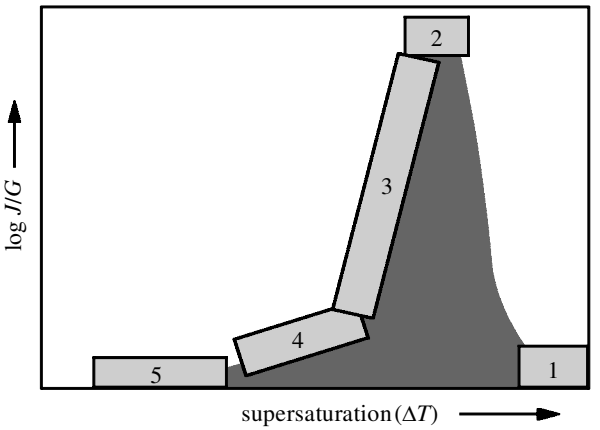

Figure 13. Schematic showing the range of plagioclase textures observed at Mt St Helens, shown in the context of figure 9*b*. Numbered boxes represent the following: 1, microlite-free pumice; 2, finely crystalline pyroclasts; 3, microphenocryst-bearing pumice; 4, microphenocryst-bearing lava; 5, plagioclase phenocrysts (Cashman 1988).

were low (less than 0.05 mm^{-3} s) and crystallization times long (at least weeks). At these conditions, ΔT would be low, and crystal growth would dominate the crystallization process. Thus it appears that the range in plagioclase textures observed in products of the 1980–1986 eruption of Mt St Helens can be directly related to the decompression history of individual samples, and the resulting J/G history experienced (figure 13). When the phenocryst population is also considered, the observed textures describe most of the theoretical J/G curve shown in figure 9*b*.

(iii) *Mt Spurr, 1992*

The examples above rely heavily on observational and monitoring data for interpretation of groundmass textures. However, the extreme sensitivity of microlite textures to changes in decompression paths suggests that pyroclast textures may preserve information on subtle changes in ascent conditions that cannot yet be measured directly. A possible example is the 1992 eruption of Mt Spurr, Alaska. This eruption comprised three separate explosive events, each of 3–4 h duration, and each producing $12–15 \times 10^6$ m^3 of homogeneous mafic andesite (Keith 1995). Fallout tephra from each event showed a range of clast colours (tan to grey) and densities (980–2700 kg m^{-3} (Neal *et al.* 1995)). All clasts had abundant microlites of plagioclase, pyroxene, and Fe–Ti oxides, although microlite abundance was higher in the high-density grey clasts than in the low-density tan clasts. That crystallization occurred during, rather than before, eruption is suggested by (1) the repeatability of textural trends (including increasing groundmass crystallinity through each eruptive episode) despite differing pre-eruptive repose intervals; (2) the absence of microlite-free pyroclasts; (3) the large vertical distance (5–10 km) required to supply the volume of magma erupted, assuming a reasonable conduit radius (20–30 m); and (4) the absence of hornblende breakdown or other indications of shallow magma storage (Gardner *et al.* 1998*a*).

Sequentially erupted pyroclasts show temporal changes in microlite textures that can be related to changes in eruption dynamics (Gardner *et al.* 1998*a*). For example, plagioclase number densities in clasts from the June 1992 eruption increased by an

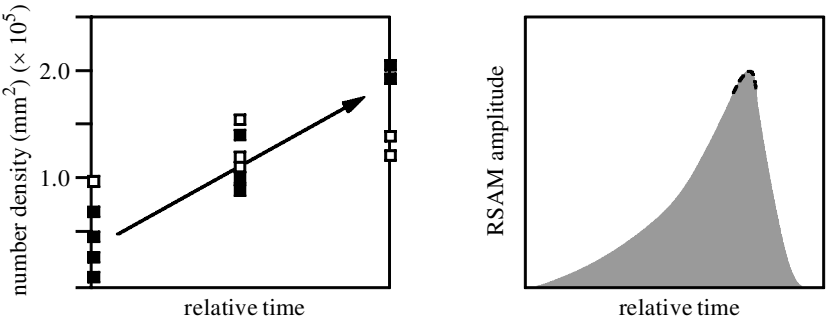

Figure 14. Comparison of plagioclase number density and seismic amplitude (RSAM) variations with time through the June 1992 eruption of Mt Spurr (redrafted from Gardner *et al.* (1998*a*)). Solid squares denote 'grey' pumice, while open squares denote 'tan' pumice.

order of magnitude (10^6–10^7 mm^{-3}) during the 4 h of eruptive activity, apparently reflecting an increase in mass flux, as indicated by seismic amplitude (RSAM) records (figure 14). The 4–19 h of seismicity preceding this eruption, combined with the 4 h duration of the eruption itself, provide bracketing decompression times and resulting nucleation (15–500 mm^{-3} s) and growth (1.5–50 $\times 10^{-8}$ mm s^{-1}) rates (table 1). Crystallization was extensive, as illustrated by total groundmass crystallinities of up to 80%. Rare holocrystalline clasts produced during the last (September 1992) eruptive event also suggest efficient syn-ascent crystallization of Spurr magma. Thus anomalously elevated post-eruption seismicity (Power *et al.* 1995) may be interpreted as a reflection of extensive crystallization within the conduit as a consequence of waning ascent rates, 'freezing' the magma and inhibiting further ascent (Cashman *et al.* 1998; Gardner *et al.* 1998*a*).

(*c*) *Textures' summary*

Crystal textures (size, abundance, and to a lesser extent shape) are influenced by the ΔT (J/G) regime in which they formed. Undercooling, in turn, can be linked to the rate and path of magma decompression through the appropriate phase diagram (e.g. figure 1). Examples provided from Pinatubo (figure 10), Mt St Helens (figure 12), and Mt Spurr (figure 13) show that simple measurement of crystal number density (N_a or N_v) can be used to track changes in the parameter J/G (equation (4.1)), and thus provide qualitative information on changes in ΔT. Together these studies permit us to define relationships among crystal number density, relative degree of undercooling, and eruptive style.

In magmas of intermediate bulk composition, suppression of syn-eruptive crystallization requires rapid decompression and eruption. Rapid decompression followed by temporary magma arrest at shallow levels results in extensive crystallization, often of both feldspar and an Si-phase. Moderate rates of decompression, in contrast, produce less numerous but larger plagioclase microphenocrysts. Controls on crystal growth may be further defined if crystal size and shape distributions are also determined (Hammer *et al.* 1999). Taken together, these studies suggest that the decompression path determines the resulting groundmass texture, and that better constraints on relationships between decompression rate and effective ΔT in melts of different com-

positions would substantially improve the quantitative interpretation of groundmass textures.

Bulk rates and extents of groundmass crystallization are higher in the more mafic Spurr magma (andesitic melt) than in the rhyodacitic and rhyolitic melts of Mt St Helens and Pinatubo (table 1). Additionally, the Spurr eruption produced no microlite-free pyroclasts, although each eruptive event was of similar (or greater) magnitude and duration as explosive eruptions at Mt St Helens that produced microlite-free pumice. These observations suggest a strong compositional control on syn-eruptive crystallization, and permit the following speculations. Low microlite contents characterize effusively erupted obsidian domes (less than 1% (Swanson *et al*. 1989; Sharp *et al*. 1996; Manga 1998)), despite assumed low rates of ascent (long decompression times). Thus the kinetic lag time for crystallization in these highly viscous melts is long relative to magma rise times. In contrast, the highly crystalline pyroclasts produced during explosive eruption of Mt Spurr suggest that hydrous magmas of basaltic andesite (and basalt) compositions may be unable to ascend volcanic conduits sufficiently rapidly to prevent decompression-driven crystallization. Magmas of dacitic compositions are intermediate between these two extremes, and thus produce clasts with crystallinities that depend on the exact decompression path. As high crystallinities result in both high viscosities and non-Newtonian rheologies of the resultant magma (Pinkerton & Stevenson 1992; Lejeune & Richet 1995), we might expect explosive style to change with increasing syn-eruptive crystallization. For example, the Vulcanian activity that commonly initiates eruptions results from the formation of a solid (partly crystallized) plug within the conduit that temporarily seals the system and thus serves to modulate explosive activity. The extrusion of Peléean spines also reflects extensive decompression-driven crystallization accompanying very slow rates of magma ascent. On a more speculative note, the inception or termination of eruptions with phreatomagmatic activity may reflect conditions where decompression-induced crystallization produced sufficiently high magma viscosities to change pressure gradients within the conduit, and thus permit entrance of external water (Cashman *et al*. 1998; Gardner *et al*. 1998*a*, *b*).

5. Summary

Crystallization is an unavoidable consequence of decompressing a water-saturated melt, provided that there is sufficient time to overcome kinetic delays to crystallization. The addition of crystals to a melt will, in turn, change magma rheology and thus affect the rate of continued magma ascent and eruption. Both matrix melt composition and groundmass crystallinity change as a result of crystallization, and can thus be used to determine time-scales of magma ascent. Relative (quartz-undersaturated) and absolute (quartz-saturated) melt equilibration pressures may be determined from projection of glass compositions onto the Qz–Ab–Or ternary. These compositions can be correlated with rates of magma ascent. Crystal textures also record conditions of magma decompression. Particularly informative is crystal number density, a direct measure of the relative importance of nucleation and growth during crystallization, which in turn is indicative of effective undercooling. Finally, recent work on phenocryst growth in water-rich basaltic magmas has suggested that much of the crystallization may occur rapidly, as a consequence of decompression (Sisson & Grove 1993*a*; Brophy *et al*. 1999; Kuritani 1999). It seems likely that decompression-

related crystallization may also be responsible for much of the phenocryst, formation (particularly plagioclase) observed in andesitic magmas (Blundy & Cashman 2000). Thus the entire population of crystals in a pumice or lava sample may preserve, in remarkable detail, much of the decompression history of the magma.

This work was supported by NSF EAR9614753 (to K.C.). J.D. thanks The Royal Society for a Research Fellowship and the Fulbright Commission for partial support of a sabbatical visit to the University of Oregon. Reviews from S. Sparks and C. Jaupart helped to clarify the text substantially and are gratefully acknowledged.

References

Alidibirov, M. & Dingwell, D. B. 1996 Magma fragmentation by rapid decompression. *Nature* **380**, 146–148.

Armienti, P., Pareschi, M. T., Innocenti, F. & Pompilio, M. 1994 Effects of magma storage and ascent on the kinetics of crystal growth. *Contrib. Mineral. Petrol.* **115**, 402–414.

Barclay, J., Rutherford, M. J., Carroll, M. R., Murphy, M. D., Devine, J. D., Gardner, J. & Sparks, R. S. J. 1998 Experimental phase equilibria constraints on pre-eruptive storage conditions of the Soufrière Hills magma. *Geophys. Res. Lett.* **25**, 3437–3440.

Baxter, P. J. (and 11 others) 1999 Cristobalite in volcanic ash of the Soufrière Hills volcano, Montserrat: hazards and implications. *Science* **283**, 1142–1145.

Bernard, A., Knittel, U., Weber, B., Weis, D., Albrecht, A., Hattori, K., Klein, J. & Oles, D. 1996 Petrology and geochemistry of the 1991 eruption products of Mount Pinatubo. In *Fire and mud* (ed. C. G. Newhall & R. Punongbayan), pp. 767–798. Seattle: University of Washington Press.

Blatter, D. & Carmichael, I. 1998 Plagioclase-free andesites from Zitacuro (Michoacan), Mexico: petrology and experimental constraints. *Contrib. Mineral. Petrol.* **132**, 121–138.

Blundy, J. & Cashman, K. 2000 Magma ascent and crystallisation at Mount St. Helens, 1980–1986. *Contrib. Mineral. Petrol.* (In the press.)

Brandeis, G. & Jaupert, C. 1987 The kinetics of nucleation and crystal growth and scaling laws for magmatic crystallization. *Contrib. Mineral. Petrol.* **96**, 24–34.

Brophy, J. G., Whittington, C. S. & Park, Y.-R. 1999 Sector-zoned augite megacrysts in Aleutian high alumina basalts: implications for the conditions of basalt crystallization and the generation of calc-alkaline series magmas. *Contrib. Mineral. Petrol.* **135**, 277–290.

Burnham, C. W. 1979 The importance of volatile constituents. In *The evolution of the igneous rocks: fiftieth anniversary perspectives* (ed. H. S. Yoder), pp. 439–482. Princeton University Press.

Cashman, K. V. 1988 Crystallization of Mount St. Helens dacite: a quantitative textural approach. *Bull. Volcanol.* **50**, 194–209.

Cashman, K. V. 1990 Textural constraints on the kinetics of crystallization of igneous rocks. *Rev. Mineral.* **24**, 259–314.

Cashman, K. V. 1992 Groundmass crystallization of Mount St. Helens dacite, 1980–1986: a tool for interpreting shallow magmatic processes. *Contrib. Mineral. Petrol.* **109**, 431–449.

Cashman, K. V. 1993 Relationship between plagioclase crystallization and cooling rate in basaltic melts. *Contrib. Mineral. Petrol.* **113**, 126–142.

Cashman, K. V. & Taggart, J. E. 1983 Petrologic monitoring of 1981 and 1982 eruptive products from Mount St. Helens. *Science* **221**, 1385–1387.

Cashman, K., Gardner, C., Power, J. & Houghton, B. 1998 Recent Cook Inlet eruptions. 1. Lava effusion and eruption terminations. *Eos* **79**, 1000.

Cashman, K., Thornber, C. & Kauahikaua, J. 1999 Cooling and crystallization of lava in open channels, and the transition of pahoehoe lava to `a`a. *Bull. Volcanol.* **61**, 306–323.

Chayes, F. 1956 *Petrographic modal analysis*. Wiley.

Criswell, C. W. 1987 Chronology and pyroclastic stratigraphy of the May 18, 1980 eruption of Mount St. Helens, Washington. *J. Geophys. Res.* **92**, 10 237–10 266.

Devine, J. D., Rutherford, M. J. & Gardner, J. E. 1998*a* Petrologic determination of ascent rates for the 1995–1997 Soufrière Hill volcano andesitic magma. *Geophys. Res. Lett.* **25**, 3673–3676.

Devine, J., Murphy, M., Rutherford, M., Barclay, J., Sparks, R., Carroll, M., Young, S. & Gardner, J. 1998*b* Petrologic evidence for pre-eruptive pressure–temperature conditions, and recent reheating, of andesitic magma erupting at the Soufrière Hills volcano, Montserrat, W.I. *Geophys. Res. Lett.* **25**, 3669–3672.

Endo, E. T., Dzurisin, D. & Swanson, D. A. 1990 Geophysical and observational constraints for ascent rates of dacitic magma at Mount St. Helens. In *Magma transport and storage* (ed. M. P. Ryan), pp. 318–334. Wiley.

Gardner, C. A., Cashman, K. V. & Neal, C. A. 1998*a* Tephra-fall deposits from the 1992 eruption of Crater Peak, Alaska: implications of clast textures for eruptive processes. *Bull. Volcanol.* **59**, 537–555.

Gardner, C. A., Cashman, K. V. & Power, J. 1998*b* Recent Cook Inlet eruptions. 2. Degassing-induced crystallization and eruption inception. *Eos* **79**, 1000.

Geschwind, C.-H. & Rutherford, M. J. 1995 Crystallization of microlites during magma ascent: the fluid mechanics of 1980–1986 eruptions at Mount St. Helens. *Bull. Volcanol.* **57**, 356–370.

Gilbert, J. S. & Sparks, R. S. J. (eds) 1998 Future research directions on the physics of explosive volcanic eruptions. In *The physics of explosive volcanic eruptions. Geol. Soc. Lond. Spec. Publ.* **145**, 1–7.

Grove, T. L., Donnelly-Nolan, J. M. & Housh, T. 1997 Magmatic processes that generated the rhyolite of Glass Mountain, Medicine Lake Volcano, N. California. *Contrib. Mineral. Petrol.* **127**, 205–223.

Hammer, J. & Rutherford, M. 1999 Kinetics of decompression-induced crystallization in H_2O-rich dacite. *Eos* **80**, 1128.

Hammer, J. E., Cashman, K. V., Hoblitt, R. & Newman, S. 1999 Degassing and microlite crystallization during the pre-climactic events of the 1991 eruption of the Mt. Pinatubo, Phillipines. *Bull. Volcanol.* **60**, 355–380.

Hammer, J. E., Cashman, K. V. & Voight, B. 2000 Magmatic processes revealed by textural and compositional trends in Merapi dome lavas. *J. Volcanol. Geotherm. Res.* (In the press.)

Hess, K.-U. & Dingwell, D. B. 1996 Viscosities of hydrous leucogranitic melts: a non-Arrhenian model. *Am. Mineral.* **81**, 297–304.

Higgins, M. 1994 Numerical modeling of crystal shapes in thin sections: estimation of crystal habit and true size. *Am. Mineral.* **79**, 113–119.

Higgins, M. 1996*a* Crystal size distributions and other quantitative textural measurements in lavas and tuff from Egmont volcano (Mt. Taranaki), New Zealand. *Bull. Volcanol.* **58**, 194–204.

Higgins, M. 1996*b* Magma dynamics beneath the Kameni volcano, Greece, as revealed by crystal size and shape measurements. *J. Volcanol. Geotherm. Res.* **70**, 37–48.

Hoblitt, R. P. & Harmon, R. S. 1993 Bimodal density distribution of cryptodome dacite from the 1980 eruption of Mount St. Helens, Washington. *Bull. Volcanol.* **55**, 421–437.

Hoblitt, R. P., Wolfe, E. W., Scott, W. E., Couchman, M. R., Pallister, J. S. & Javier, D. 1996 The preclimactic eruptions of Mount Pinatubo, June 1991. In *Fire and mud* (ed. C. G. Newhall & R. Punongbayan), pp. 457–512. Seattle: University of Washington Press.

Holtz, F., Pichavant, M., Barbey, P. & Johannes, W. 1992*a* Effects of H_2O on the liquidus phase relations in the haplogranitic system at 2 and 5 kbar. *Am. Mineral.* **77**, 1223–1241.

Holtz, F., Johannes, W. & Pichavant, M. 1992*b* Effect of excess aluminum on phase relations in the system Qz–Ab–Or. Experimental investigations at 2 kbar and reduced H_2O-activity. *Eur. J. Mineral.* **4**, 137–152.

Jaupart, C. 1998 Gas loss from magmas through conduit walls during eruption. In *The physics of explosive volcanic eruptions* (ed. J. S. Gilbert & R. S. J. Sparks). *Geol. Soc. Spec. Publ.* **145**, 73–90.

Johannes, W. 1980 Metastable melting in the granite system Qz–Ab–Or–An–H_2O. *Contrib. Mineral. Petrol.* **72**, 73–80.

Johannes, W. & Holtz, F. 1996 *Petrogenesis and experimental petrology of granitic rocks.* Springer.

Keith, T. E. C. (ed.) 1995 The 1992 Eruptions of Crater Peak Vent, Mount Spurr Volcano, Alaska. *US Geol. Surv. Bull.* **2139**, 1–220.

Kirkpatrick, R. J. 1981 Kinetics of crystallization of igneous rocks. *Rev. Mineral.* **8**, 321–398.

Klug, C. & Cashman, K. V. 1994 Vesiculation of May 18, 1980 Mount St. Helens magma. *Geology* **22**, 468–472.

Kuntz, M. A., Rowley, P. D., MacLeod, N. S., Reynolds, R. L., MacBroome, L. A., Kaplan, A. M. & Lidke, D. J. 1981 Petrography and particle-size distribution of pyroclastic-flow, ash-cloud, and surge deposits. *US Geol. Surv. Prof. Paper* **1250**, 525–539.

Kuritani, T. 1999 Phenocryst crystallization during ascent of alkali basalt magma at Rishiri volcano, northern Japan. *J. Volcanol. Geotherm. Res.* **88**, 77–97.

Lejeune, A.-M. & Richet, P. 1995 Rheology of crystal-bearing silicate melts: an experimental study at high viscosities. *J. Geophys. Res.* **100**, 4215–4230.

Lofgren, G. E. 1980 Experimental studies on the dynamic crystallization of silicate melts. In *The physics of magmatic processes* (ed. R. B. Hargraves), pp. 487–551. Princeton.

Manga, M. 1998 Orientation distribution of microlites in obsidian. *J. Volcanol. Geotherm. Res.* **86**, 107–115.

Marsh, B. D. 1998 On the interpretation of crystal size distributions in magmatic systems. *J. Petrol.* **39**, 553–599.

Melnik, O. & Sparks, R. S. J. 1999 Nonlinear dynamics of lava dome extrusion. *Nature* **402**, 37–41.

Melson, W. G. 1983 Monitoring the 1980–1982 eruptions of Mount St. Helens: compositions and abundance of glass. *Science* **221**, 1387–1391.

Merzbacher, C. & Eggler, D. H. 1984 A magmatic geohygrometer: application to Mount St. Helens and other dacitic magmas. *Geology* **12**, 587–590.

Moore, G. & Carmichael, I. S. E. 1998 The hydrous phase equilibria (to 3 kbar) of an andesite and basaltic andesite from western Mexico: constraints on water content and conditions of phenocryst growth. *Contrib. Mineral. Petrol.* **130**, 304–319.

Moore, J. G., Lipman, P. W., Swanson, D. A. & Alpha, T. R. 1981 Growth of lava domes in the crater, June 1980–January 1981. *US Geol. Surv. Prof. Paper* **1250**, 541–547.

Moran, S. C. 1994 Seismicity at Mount St. Helens, 1987–1992; evidence for repressurization of an active magmatic system. *J. Geophys. Res.* **99**, 4341–4354.

Murphy, M. D., Sparks, R. S. J., Barclay, J., Carroll, M. R. & Brewer, T. S. 2000 Remobilisation origin for andesite magma by intrusion of mafic magma at the Soufrière Hills volcano, Montserrat, W.I. A trigger for renewed eruption. *J. Petrol.* (In the press.)

Murphy, M. D., Sparks, R., Barclay, J., Carroll, M., Lejeune, A.-M., Brewer, T., Macdonald, R., Black, S. & Young, S. 1998 The role of magma mixing in triggering the current eruption at the Soufrière Hills volcano, Montserrat, West Indies. *Geophys. Res. Lett.* **25**, 3433–3436.

Nakada, S. & Motomura, Y. 1999 Petrology of the 1991–1995 eruption at Unzen: effusion pulsation and groundmass crystallization. *J. Volcanol. Geotherm. Res.* **89**, 173–196.

Nakada, S., Motomura, Y. & Shimizu, H. 1995 Manner of magma ascent at Unzen Volcano (Japan). *Geophys. Res. Lett.* **22**, 567–570.

Navon, O., Chekhmir, A. & Lyakhovsky, V. 1998 Bubble growth in highly viscous melts: theory, experiments, and autoexplosivity of dome lavas. *Earth Planet. Sci. Lett.* **160**, 763–776.

Neal, C. A. McGimsey, R. G., Gardner, C. A., Harbin, M. L. & Nye, C. J. 1995 Tephra-fall deposits from the 1992 eruptions of Crater Peak, Mount Spurr Volcano, Alaska; a preliminary report on distribution, stratigraphy, and composition. In *The 1992 eruptions of Crater Peak Vent, Mount Spurr Volcano, Alaska* (ed. T. E. C. Keith). *US Geol. Surv. Bull.* **2139**, 65–79.

Pallister, J. S., Hoblitt, R. P., Meeker, G. P., Knight, R. J. & Siems, D. F. 1996 Magma mixing at Mount Pinatubo; petrographic and chemical evidence from the 1991 deposits. In *Fire and mud* (ed. C. G. Newhall & R. Punongbayan), pp. 687–731. Seattle: University of Washington Press.

Pinkerton, H. & Stevenson, R. J. 1992 Methods of determining the rheological properies of magmas at sub-liquidus temperatures. *J. Volcanol. Geotherm. Res.* **53**, 47–66.

Power, J. A., Jolly, A. D., Page, R. A. & McNutt, S. R. 1995 Seismicity and forecasting of the 1992 eruptions of Crater Peak vent, Mount Spurr volcano, Alaska. In *The 1992 eruptions of Crater Peak Vent, Mount Spurr Volcano, Alaska* (ed. T. E. C. Keith). *US Geol. Surv. Bull.* **2139**, 149–159.

Rutherford, M. D. & Devine, J. D. 1988 The May 18, 1980 eruption of Mount St. Helens. 3. Stability and chemistry of amphibole in the magma chamber. *J. Geophys. Res.* **93**, 11 949–11 959.

Rutherford, M. J. & Devine, J. D. 1996 Pre-eruption pressure–temperature conditions and volatiles in the 1991 dacitic magma of Mount Pinatubo In *Fire and mud* (ed. C. G. Newhall & R. Punongbayan), pp. 751–766. Seattle: University of Washington Press.

Rutherford, M. J. & Hill, P. M. 1993 Magma ascent rates from amphibole breakdown: an experimental study applied to the 1980–1986 Mount St. Helens eruption. *J. Geophys. Res.* **98**, 19 667–19 686.

Rutherford, M. D., Sigurdsson, H., Carey, S. & Davis, A. 1985 The May 18, 1980 eruption of Mount St. Helens. 1. Melt composition and experimental phase equilibria. *J. Geophys. Res.* **90**, 2929–2947.

Sato, H., Nakada, S., Fujii, T., Nakamura, M. & Suzuki-Kamata, K. 1999 Groundmass pargasite in the 1991–1995 dacite of Unzen volcano: phase stability experiments and volcanological implications. *J. Volcanol. Geotherm. Res.* **89**, 197–212.

Scandone, R. & Malone, S. D. 1985 Magma supply, magma discharge and readjustment of the feeding system of Mount St. Helens during 1980. *J. Volcanol. Geotherm. Res.* **23**, 239–262.

Schairer, J. F. 1950 The alkali feldspar join in the system $NaAlSiO_4$–$KAlSiO_4$–SiO_4. *J. Geol.* **58**, 512–517.

Sharp, T. G. Stevenson, R. J. & Dingwell, D. B. 1996 Microlites and 'nanolites' in rhyolitic glass; microstructural and chemical characterization. *Bull. Volcanol.* **57**, 631–640.

Shaw, H. 1965 Comments on viscosity, crystal settling and convection in granitic magmas. *Am. J. Sci.* **263**, 120–152.

Sisson, T. W. & Grove, T. L. 1993*a* Experimental investigations of the role of H_2O in calc-alkaline differentiation and subduction zone magmatism. *Contrib. Mineral. Petrol.* **113**, 143–166.

Sisson, T. W. & Grove, T. L. 1993*b* Temperatures and H_2O contents of low-MgO high-alumina basalts. *Contrib. Mineral. Petrol.* **113**, 167–184.

Sparks, R. S. J. 1997 Causes and consequences of pressurization in lava dome eruptions. *Earth Planet. Sci. Lett.* **150**, 177–189.

Sparks, R. S. J. (and 17 others) 1998 Magma production and growth of the lava dome of the Soufrière Hills volcano, Montserrat, West Indies: November 1995 to December 1997. *Geophys. Res. Lett.* **25**, 3421–3424.

Stix, J., Torres, R. C., Narvaez, L. M., Cortes, G. P. J., Raigosa, J. A., Gomez, D. M. & Castonguay, R. 1997 A model of vulcanian eruptions at Galeras volcano, Columbia. *J. Volcanol. Geotherm. Res.* **77**, 285–303.

Swanson, D. A., Dzurisin, D. R. T. H., Iwatsubo, E. Y., Chadwick, W. W., Casadevall, T. J., Ewert, J. W. & Heliker, C. C. 1987 Growth of the lava dome at Mount St. Helens, Washington, 1981–1983. *Geol. Soc. Am. Special Paper* **212**, 1–16.

Swanson, S. E., Naney, M. T., Westrich, H. R. & Eichelberger, J. C. 1989 Crystallization history of Obsidian Dome, Inyo Domes, California. *Bull. Volcanol.* **51**, 161–176.

Tuttle, O. F. & Bowen, N. L. 1958 Origin of granite in the light of experimental studies in the system $NaAlSi_3O_8$–$KAlSi_3O_8$–SiO_2–H_2O. *Geol. Soc. Am. Mem.* **74**, 153 pp.

Underwood, E. 1970 *Quantitative stereology*. Addison-Wesley.

Venezsky, D. & Rutherford, M. 1999 Petrology and Fe–Ti oxide reequilibration of the 1991 Mount Unzen mixed magma. *J. Volcanol. Geotherm. Res.* **89**, 213–230.

Winkler, H. 1949 Crystallization of basaltic magma as recorded by variation of crystal size in dikes. *Mineral Mag.* **28**, 557–574.

Wolf, K. J. & Eichelberger, J. C. 1997 Syneruptive mixing, degassing and crystallization at Redoubt volcano, eruption of December 1989 to May 1990. *J. Volcanol. Geotherm. Res.* **75**, 19–37.

Yoder, H. S. 1968 Albite–anorthite–quartz–water at 5 kbar. *Carnegie Inst. Wash. Yearbk* **66**, 477–478.

Young, S., Sparks, R. S., Aspinall, W. P., Lynch, L., Miller, A. D., Robertson, R. E. A. & Shepherd, J. B. 1998 Overview of the eruption of Soufrière Hills volcano, Monserrat, 18 July 1995 to December 1997. *Geophys. Res. Lett.* **25**, 3389–3392.

PHILOSOPHICAL TRANSACTIONS OF THE ROYAL SOCIETY A MATHEMATICAL, PHYSICAL & ENGINEERING SCIENCES